

Chapter 3.

A versatile cis-blocking strategy for ribozyme characterization

Abstract

Synthetic RNA control devices that utilize ribozyme-based actuator components have been demonstrated in diverse organisms to regulate cellular behaviors in response to environmental signals. The quantitative measurements of the *in vitro* cleavage rates associated with these synthetic devices are essential for advancing our understanding of the corresponding *in vivo* gene-regulatory activities. One of the key challenges in the ribozyme characterization is the efficient generation of full-length RNA through transcription reactions. Current methods of full-length RNA generation require a laborious gel purification step. We developed a cis-blocking strategy that supports efficient generation of full-length RNA by a simple gel-free process. We demonstrated that our cis-blocking strategy is applicable to both natural ribozymes and synthetic ribozyme devices. The cleavage rates obtained on the full-length RNA generated from the cis-blocking strategy were characterized and closely correlated to those from the trans-blocking strategy. We further developed a rapid, label-free cleavage assay based on surface plasmon resonance (SPR). The SPR-based assay allows rapid monitoring of ribozyme cleavage under varying reaction conditions. With further optimization and development, our cis-blocking and SPR-based characterization strategies will provide a powerful method for ribozyme characterization.

3.1 INTRODUCTION

Synthetic biology is advancing the design of genetic circuits encoding desired functions (1). As the proper functioning of synthetic genetic circuits often relies on the precise control and tuning of key protein component levels, much effort in the field has focused on developing programmable gene-regulatory devices. One class of gene-regulatory devices, so called RNA control devices, utilize RNA molecules to link changes in molecular signals to gene expression events. Progress in the fields of RNA biology and engineering have allowed construction of RNA control devices through the assembly of natural or synthetic components that encode more basic functions, such as sensing, information transmission, and actuation (2). Because hammerhead ribozymes can exhibit activity independent of cell-specific machinery, RNA control devices that utilize ribozyme-based actuator components have been demonstrated in diverse organisms spanning from bacterial, yeast, and mammalian systems to regulate cellular behaviors in response to one or more environmental signals (3-6).

We recently described a modular ribozyme device platform based on the functional coupling of three distinct components: an actuator encoded by a hammerhead ribozyme from satellite RNA of tobacco ringspot virus (sTRSV), a sensor encoded by an RNA aptamer, and an information transmitter encoded by a sequence capable of a programmed strand-displacement event (3) (Figure 3.1). The transmitter component directs the device to partition between two primary functional conformations, where the aptamer-folded conformation can be associated with the disruption or restoration of the ribozyme catalytic core to construct ON (increased gene expression) or OFF (decreased gene expression) devices, respectively, in response to ligand binding to the aptamer. The

quantitative tuning of device regulatory dynamic range, which is set by the gene expression activity in the absence and presence of input ligand, has been demonstrated to be important for achieving effective control over phenotypic behaviors (see Chapter 2). Computational models of ribozyme devices have predicted that the values of the ribozyme cleavage rate can have substantial impact on the device gene-regulatory activities (7). Therefore, quantitative measurements of the ribozyme cleavage rates are essential to advance our understanding of the relationship between the *in vitro* cleavage rates and the corresponding *in vivo* gene-regulatory activities.

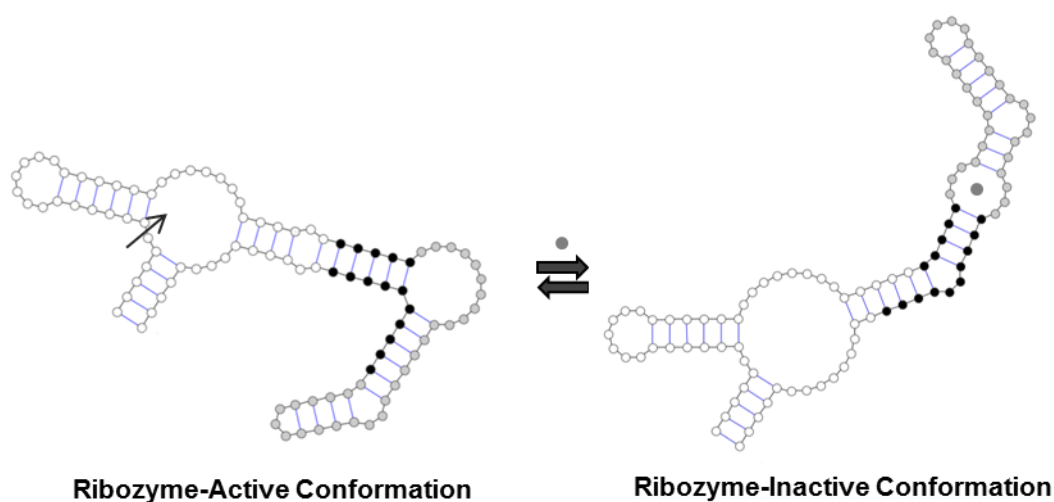


Figure 3.1 Modular composition of a synthetic ribozyme device. The ribozyme device is constructed by linking a RNA aptamer (indicated in grey) to a hammerhead ribozyme (indicated in white) through a programmed sequence (indicated in black) that directs a strand-displacement event. The device can adopt two primary functional conformations, in which the ribozyme-active conformation is associated with either aptamer-unformed or aptamer-formed conformation to construct a ribozyme ON or OFF device, respectively. In the case of a ribozyme ON device (depicted here), the device adopts a ribozyme-active conformation in the absence of the input ligand, thereby leading to self-cleavage. In the presence of the input ligand, binding of the ligand to the aptamer stabilizes a device conformation in which the ribozyme catalytic core is disrupted, thus resulting in no cleavage. Secondary structures were rendered using VARNA software (8).

A key challenge in characterizing ribozyme cleavage rates is in the efficient generation of full-length RNA for ribozyme constructs, including natural ribozymes and synthetic ribozyme devices, by *in vitro* T7 transcription reactions. Typical transcription reactions require high MgCl_2 (~mM) to achieve sufficient yield, conditions at which most ribozyme constructs exhibit high cleavage activity, thereby resulting in low yield of full-length RNA for the downstream kinetic analysis. In early characterization studies of natural ribozymes, researchers split the whole ribozyme sequence into an enzyme and a substrate strand (9,10). The two strands were transcribed separately and annealed to generate the functional two-stranded ribozyme complex. One disadvantage of this strategy is that experimental conditions need to be optimized to ensure that the measured cleavage rate is not affected by the association step between the two strands (11). Later, researchers developed a trans-blocking strategy to generate full-length single-stranded ribozyme transcripts by transcription reactions in the presence of an antisense DNA strand complementary to the ribozyme catalytic core. Full-length trans-blocked RNA was purified through polyacrylamide gel electrophoresis (PAGE) under denaturing conditions and renatured prior to cleavage assays (9,12). Although this strategy allows characterization of a ribozyme in its native conformation, previous studies have shown that the gel-purified full-length RNA was still capable of cleaving during sample handling, resulting in an ~30% loss prior to cleavage assays, and ~50% of the remaining full-length RNA does not exhibit cleavage activity (9). Therefore, a more efficient ribozyme-blocking strategy is desired.

As the kinetics of ribozyme cleavage are slow relative to many protein enzymes, ribozyme cleavage rates are typically measured through a gel electrophoretic separation

method (11,12). The cleavage reaction is initiated by the addition of $MgCl_2$ to the radiolabelled full-length RNA and quenched at different time points. The quenched samples are resolved by denaturing PAGE to determine the fraction RNA cleaved as a function of time, which are fit to a first-order exponential equation to obtain the cleavage rate. Because the gel-based ribozyme cleavage assay is discontinuous, several time points are required in the initial as well as the final phase of the reaction for proper analysis, thereby making the gel-based assay a time-consuming process. A continuous ribozyme cleavage assay based on the intramolecular fluorescence resonance energy transfer (FRET) has been developed and applied to characterize ribozyme cleavage rates (13,14). However, the FRET-based cleavage assay requires labeling of RNA molecules with appropriate fluorophores and is currently limited to the characterization of two-stranded ribozyme complexes only.

Advances in biosensor technologies have led to the development of the Biacore platform based on surface plasmon resonance (SPR) for real-time detection of biomolecular interactions (15). The Biacore platform utilizes a sensor surface modified with one molecule and measures the refractive index change, which is associated with the local mass density change, due to the association or dissociation of another molecule in solution. The refractive index change is converted into an SPR signal, which is expressed in resonance units (RU), and fitted to a mathematical model to acquire thermodynamic and kinetic parameters. The Biacore platform requires no labeling of molecules, consumes little sample, and is highly-automated, thus making it an attractive tool for developing novel ribozyme characterization strategies.

In this work, we developed a simple two-step gel-free process that allows efficient generation of full-length transcription products for diverse ribozyme constructs. We designed an RNA sequence that was directly incorporated into the target transcript to co-transcriptionally inhibit the formation of the ribozyme-active conformations. The catalytic activity of the RNA was restored by the use of a DNA competing strand to activate the blocked RNA through a fast toehold-mediated strand-displacement reaction. We demonstrated our cis-blocking strategy to generate full-length RNA transcripts for various natural ribozymes and synthetic ribozyme devices, with a blocking efficiency of up to ~90%. We performed gel-based cleavage assays to measure the cleavage rates of RNA generated from the cis-blocking strategy and compared these rates to those obtained from the more traditional trans-blocking strategy. The two rates were closely correlated, but further optimization of gel-based assays on RNA generated from the cis-blocking strategy is needed. Lastly, we described a label-free and real-time SPR-based ribozyme cleavage assay. Initial results suggested that the SPR-based cleavage assay can provide a rapid and quantitative alternative to the traditional gel-based assay.

3.2 RESULTS

3.2.1 A cis-acting RNA blocking sequence supports inhibition of ribozyme cleavage during transcription

To prevent ribozyme constructs from cleaving during transcription, we developed a new strategy to inhibit the formation of ribozyme-active conformation co-transcriptionally. We illustrated our strategy using a hammerhead ribozyme from satellite RNA of tobacco ringspot virus (sTRSV) as an example (Figure 3.2A). We rationally designed a 12 nt RNA blocking sequence that is complementary to part of the sTRSV

ribozyme transcript (Figure 3.2A). The RNA blocking sequence was inserted in the 5' end of the sTRSV ribozyme transcript to generate a cis-blocked sTRSV construct. As the RNA is being synthesized, the blocking sequence is capable of competitively hybridizing to the targeted ribozyme sequence, thus preventing the transcribed RNA from adopting a ribozyme-active conformation (Figure 3.2A).

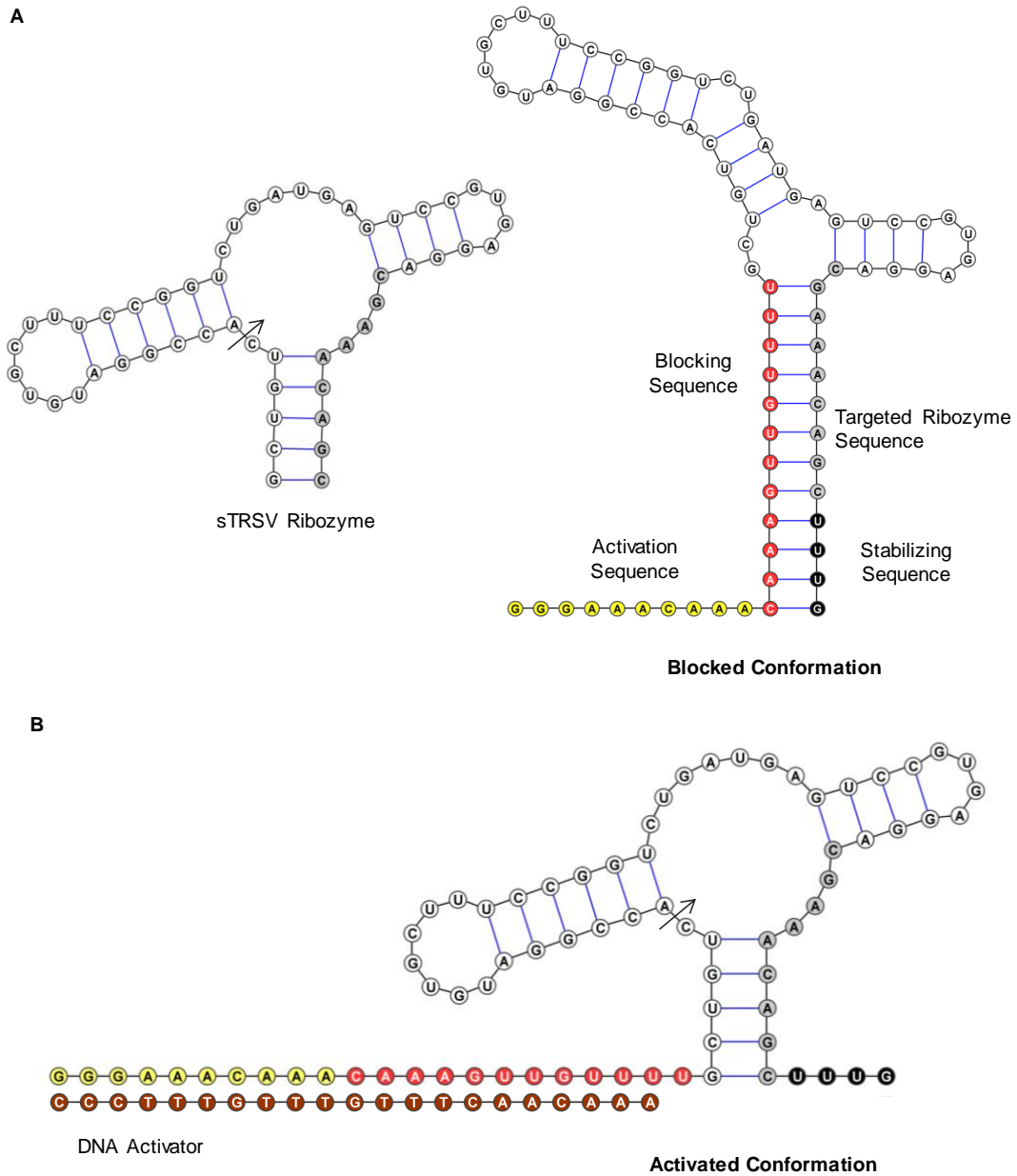


Figure 3.2 Development of the cis-blocking strategy to generate full-length RNA through transcription reactions. The cis-blocking strategy is demonstrated on a sTRSV ribozyme construct. The arrow indicates the cleavage site. (A) RNA blocking (indicated in red) and activation sequences (indicated in yellow) complementary to part of the ribozyme (indicated in grey) are directly incorporated in the 5' end of the ribozyme transcript and can inhibit the ribozyme construct from folding into the active conformation during the transcription reaction. (B) The cis-blocked ribozyme construct can be relieved by the addition of a DNA activator strand (indicated in brown), which competes with the blocking sequence to bind to the ribozyme sequence through a toehold-mediated strand-displacement reaction. As shown here, the fully hybridized ribozyme construct with the activator results in the ribozyme-active conformation. Secondary structures were predicted by RNAstructure folding software (16) and rendered using VARNA software (8).

3.2.2 A trans-acting DNA activator allows release of blocked RNA through a strand-displacement reaction

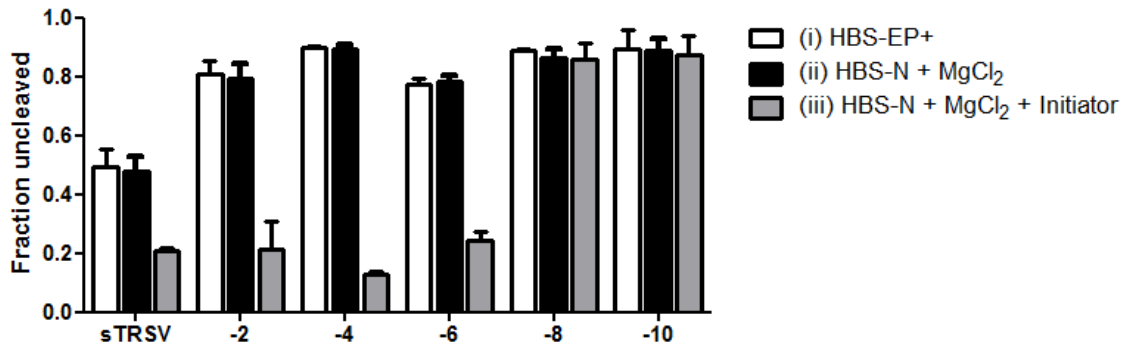
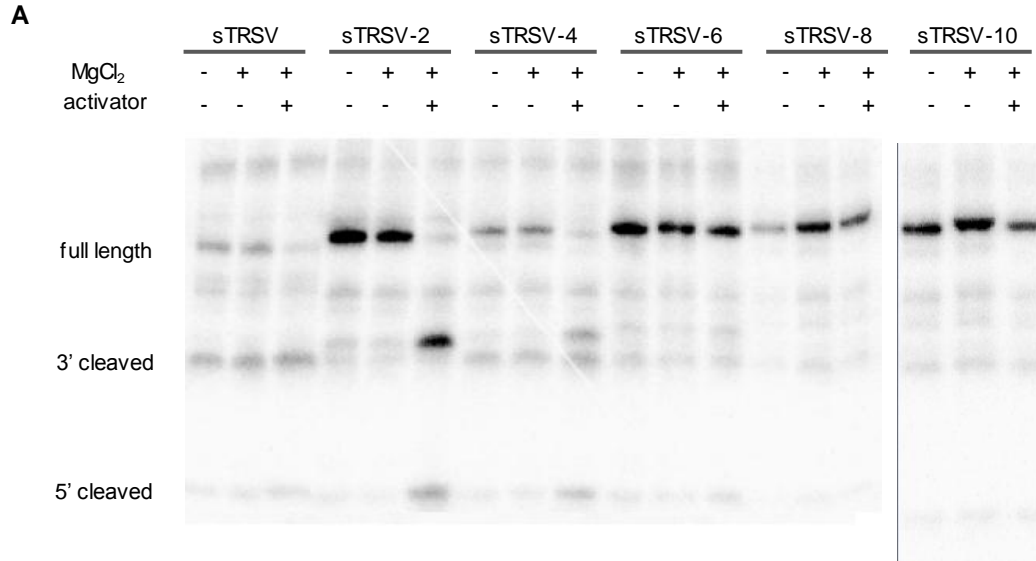
To activate the blocked sTRSV RNA for subsequent cleavage assays, we rationally designed a 10 nt RNA activation sequence as a single-stranded domain directly attached to the 5' end of the RNA blocking sequence (Figure 3.2A). The RNA activation sequence serves as a toehold to allow for the design of a DNA activator complementary to the RNA blocking sequence (Figure 3.2B). A toehold length between 5-10 nt has been demonstrated to enhance the rate of strand-displacement reaction by $\sim 10^6$ fold (17). The DNA activator can sequester the RNA blocking sequence through a fast toehold-mediated strand-displacement reaction, thus activating the blocked RNA for subsequent cleavage assays.

3.2.3 A RNA stabilizing sequence allows tuning of blocking efficiency

We tuned the strength of the competitive hybridization between the RNA blocking and targeted ribozyme sequences by introducing a stabilizing sequence at the 3' end of the sTRSV construct (Figure 3.2A). The stabilizing sequence is designed to

hybridize to the RNA activation sequence, such that the thermal stability of the blocked conformation can be tuned by varying the length of the stabilizing sequence. We increased the length of the stabilizing sequence from 4 to 14 nt to generate a variety of cis-blocked sTRSV constructs (Supplementary Figure S3.1). The blocking efficiency of the resultant sTRSV construct variants were determined by analyzing the transcription products by PAGE analysis (Figure 3.3A). By adding 4 nt to the originally designed stabilizing sequence (sTRSV-4 construct), we increased the uncleaved RNA percentage to ~90% from the transcription reaction. These results support that the cis-blocking strategy is efficient in inhibiting ribozyme cleavage during transcription.

We examined the efficacy of the toehold-mediated activation strategy by incubating the cis-blocked sTRSV construct variants at 5 mM MgCl₂ in the absence and presence of the activator strand for 30 minutes at 25°C (Figure 3.3A). In the absence of the activator strand, no cleavage was observed even at high MgCl₂, indicating that the RNA was incapable of spontaneously releasing itself from the blocked conformation. In the presence of the activator strand, however, up to ~80% of the constructs with a toehold length between 4–6 nt cleaved. Little cleavage was observed for constructs with a toehold length between 0–2 nt, suggesting that the rate of strand-displacement reaction is too slow to allow effective activation of the blocked RNA (17). These results highlight that our cis-blocking strategy is efficient in generating full-length functional RNA through two simple steps: transcription and activation.



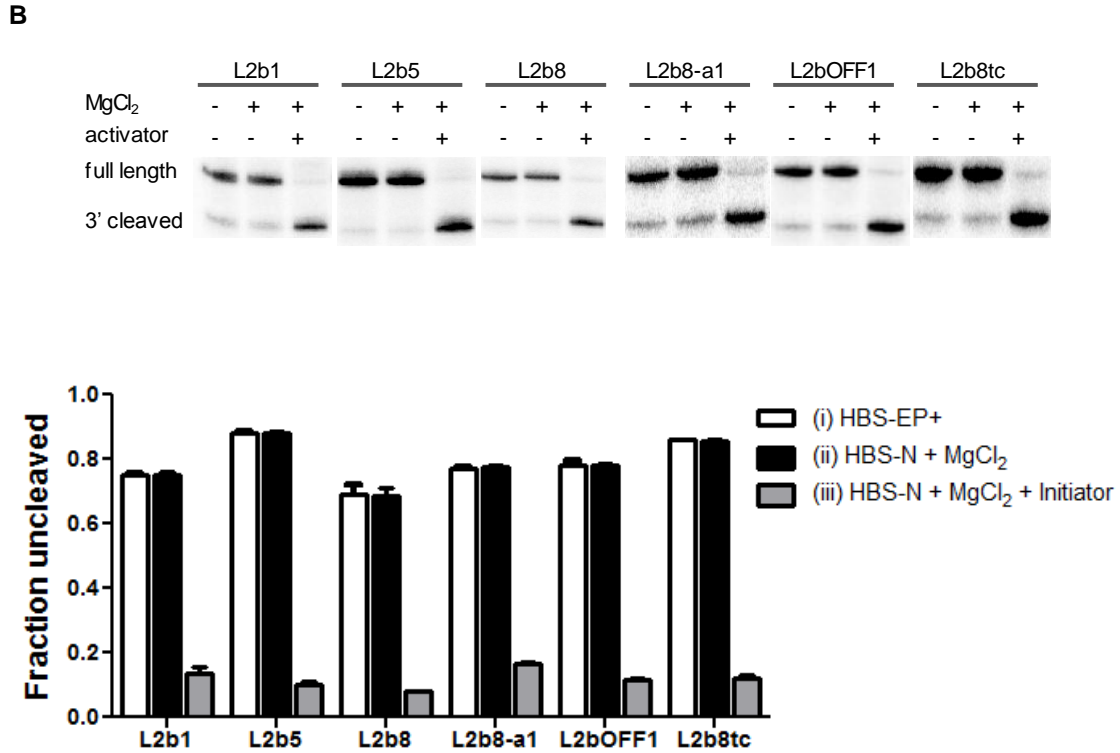


Figure 3.3 Quantification of the blocking efficiencies of the cis-blocking strategy on cis-blocked ribozyme constructs. (A) The cis-blocked sTRSV construct variants (Supplementary Figure S1) were incubated in: (i) HBS-EP buffer (10 mM HEPES, 150 mM NaCl, 3 mM EDTA, 0.05% P20, pH 7.4) (first lane); (ii) HBS-N buffer (10 mM HEPES and 150 mM NaCl, pH 7.4) in the presence of 5 mM MgCl₂ for 30 minutes at 25°C (second lane); (iii) HBS-N buffer in the presence of 5 mM MgCl₂ and 6 μM activator for 30 minutes at 25°C (third lane). The fraction of uncleaved fragment is determined through phosphorimaging analysis. A black vertical bar is used to denote samples run on different gels. (B) The blocking and activation sequences designed for the sTRSV ribozyme were directly incorporated into different synthetic ribozyme devices (L2b1, L2b5, L2b8, L2bOFF1, and L2b8tc) (Supplementary Figure S3.2). The transcription products of these constructs were analyzed as described for the cis-blocked sTRSV constructs. For clarity, only the full-length and 3' cleaved products are shown.

3.2.4 The sTRSV-blocking sequence provides a modular strategy for inhibiting cleavage of sTRSV ribozyme-based devices

Because the designed RNA blocking sequence targets only the sTRSV ribozyme, it is expected that the cis-blocking strategy can be applied to generate full-length RNA

for the sTRSV-based ribozyme devices. We inserted the RNA blocking and activation sequences in several previously characterized ribozyme devices composed of different sensors, transmitters, and actuators to generate the corresponding cis-blocked L2b1, L2b5, L2b8, L2b8-a1, L2bOFF1, and L2b8tc constructs (see Chapter 2) (Supplementary Figure S3.2). The transcription products of these constructs were diluted in HBS-EP buffer and analyzed on the gel to determine the blocking efficiencies (Figure 3.3B). Up to 90% of the total transcribed RNA was uncleaved, supporting that the RNA blocking sequence is modular to constructs based on the same ribozyme. In contrast, performing transcription reactions on a ribozyme construct without the blocking sequence resulted in significant cleavage (Supplementary Figure S3.3). The cis-blocked constructs were further incubated at 5 mM MgCl₂ in the absence and presence of the activator strand for 30 minutes at 25°C (Figure 3.3B). Similarly, the blocked constructs required both the presence of MgCl₂ and activator to cleave. Up to ~80% of the full-length blocked RNA was released by the activator and cleaved, supporting that the activation sequence optimized for the sTRSV ribozyme is modular to the corresponding ribozyme devices as well.

3.2.5 Full-length RNA generated through cis- and trans-blocking strategies exhibits comparable cleavage rates

We next examined the cleavage rates (k) measured for the full-length RNA generated from the cis-blocking strategies. The gel-based cleavage assays were performed at physiologically-relevant reaction conditions (500 μ M MgCl₂, 100 mM NaCl, and 50 mM Tris-HCl (pH 7.0)) at 37°C (Supplementary Figure S3.4). The blocked RNA was activated by incubating with the DNA activator strands prior to addition of MgCl₂. The cleavage rate constants were obtained for the L2b8 (0.063, 0.008 min⁻¹) and L2b8-a1

(0.351, 0.043 min⁻¹) constructs in the absence and presence of 5 mM theophylline, respectively (Figure 3.4A). These rates were compared to those previously obtained on the full-length RNA generated from standard trans-blocking strategies requiring PAGE purification of the blocked RNA strands (see Chapter 2) (Figure 3.4B). A correlation analysis between the cleavage rates determined through these two methods indicates a strong positive correlation (Pearson coefficient, $r = 0.9999$). However, the cleavage rates associated with the cis-blocking strategy are slower than those associated with the trans-blocking strategy. We postulate that the hybridizing reaction between the cis-blocked RNA and the activator strand may result in a slower apparent cleavage rate, thus requiring a longer incubation prior to the initiation of the cleavage reaction to allow complete activation of the RNA.

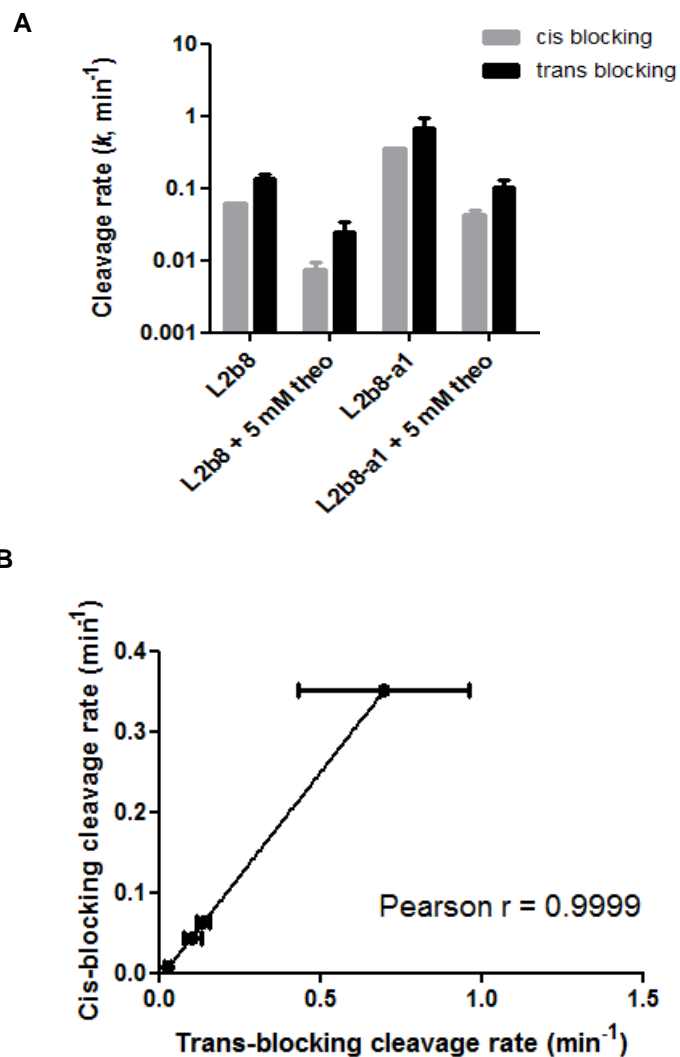


Figure 3.4 Comparison of the ribozyme cleavage rates on full-length RNA generated from different blocking strategies. (A) Gel-based cleavage assays were performed on the cis-blocked L2b8 and L2b8-a1 constructs at 37°C with 500 μ M MgCl₂, 100 mM NaCl, 50 mM Tris-HCl (pH 7.0). Cleavage rate constants (k) and errors are reported as the mean and standard deviation from at least three independent assays. The cleavage rate constants for the trans-blocked L2b8 (0.14, 0.025 min⁻¹) and L2b8-a1 (0.7, 0.1 min⁻¹) constructs were characterized previously at the same reaction conditions in the absence and presence of 5 mM theophylline, respectively (see Chapter 2). (B) Correlation analysis of cleavage rates of full-length RNA generated from the cis- and trans-blocking strategies indicates a strong correlation between these two rates; Pearson correlation coefficient (r) of 0.9999.

3.2.6 A label-free SPR-based assay to support rapid monitoring of ribozyme cleavage

Our cis-blocking and trans-activating strategies allow the development of a label-free and continuous cleavage assay based on the Biacore sensor platform (Figure 3.5). We generated a reaction sensor surface by covalently linking the DNA activator strand to the sensor surface (Figure 3.5A). The reaction sensor surface then allows both the capture and activation of the cis-blocked RNA through programmed hybridization interactions (Figure 3.5B). The capture of RNA is monitored in real time and represented as an increase in the SPR signal due to increased mass density near the sensor surface. The cleavage reaction is initiated by the injection of a buffer containing MgCl_2 (Figure 3.5C). Cleavage of the RNA results in a 3' cleaved fragment that is weakly hybridized to the immobilized DNA activator strand through five bases (14). Therefore, the 3' cleavage fragment rapidly dissociates, resulting in a decrease in the SPR signal due to decreased mass density near the sensor surface. The observed RNA dissociation rate, which reflects how fast the ribozyme construct cleaves, is obtained by fitting the sensorgram to a first-order exponential decay equation. Because the DNA-based reaction sensor surface is highly stable, the surface can be regenerated by an injection of nucleic acid denaturants (i.e., NaOH) to remove residual RNA and reused for the next cleavage assay (Figure 3.5D).

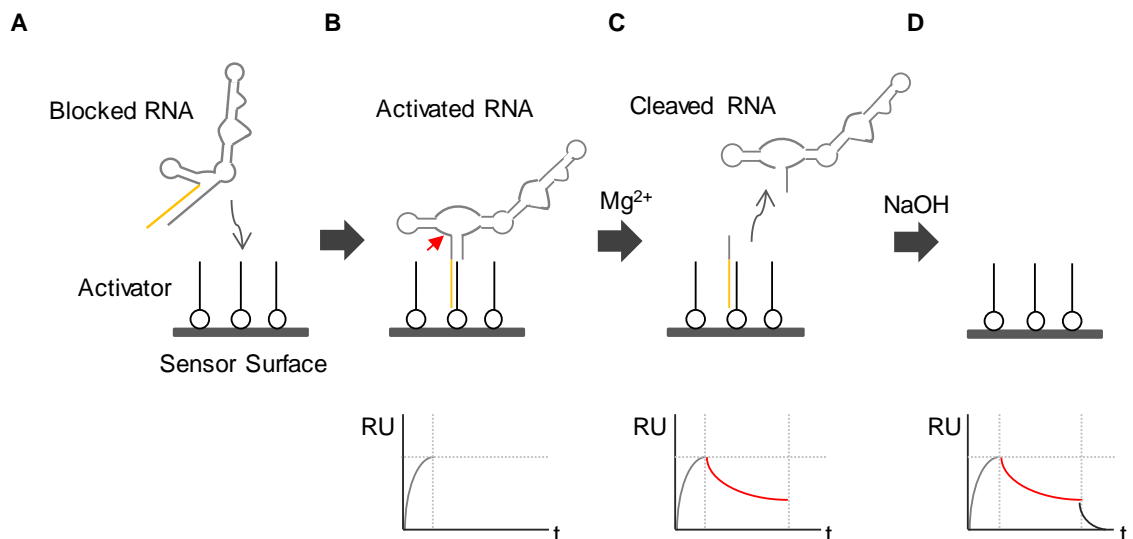


Figure 3.5 Schematic of the SPR-based ribozyme cleavage assay. (A) A sensor surface for ribozyme cleavage characterization is generated by conjugating the DNA activator strand directly to the chip surface. (B) The blocked ribozyme construct is injected over the activator-coated surface, and the hybridization interaction between the ribozyme construct and the activator, resulting in an increase in SPR signal, represented by resonance units (RU). The hybridization of the ribozyme constructs allows the activation of the blocked RNA. (C) The cleavage reaction is initiated by the injection of buffers containing $MgCl_2$ over the sensor surface. Ribozyme cleavage results in a quick dissociation of the 3' cleaved fragment, resulting in a decrease in SPR signal. The observed RNA dissociation rate is obtained by fitting the injection portion of the sensorgram to a first-order exponential decay equation (see Materials and Methods). (D) Finally, the surface is regenerated by an injection of 25 mM NaOH to remove residual RNA for the next assay.

3.2.7 The observed RNA dissociation rates are closely correlated to the cleavage rates obtained through the gel-based assay

We applied the SPR-based cleavage assays to monitor the cleavage of cis-blocked sTRSV, L2b8, and L2b8-a1 constructs under similar reaction conditions used for the gel-based cleavage assays (Supplementary Figure S3.5). The reactions were initiated by injecting buffers (500 μ M $MgCl_2$, 100 mM NaCl, and 50 mM Tris-HCl (pH 7.0)) containing: (i) no $MgCl_2$; (ii) 500 μ M $MgCl_2$; and (iii) 500 μ M $MgCl_2$ and 5 mM

theophylline (Figure 3.6A). Previous ribozyme kinetic studies have demonstrated that much higher NaCl concentrations (>4 M) are required for ribozymes to exhibit cleavage activities (18). Thus, the ribozyme constructs are expected to exhibit little cleavage activity in the absence of MgCl₂ (reaction condition (i)), and the decrease in SPR signal over the course of injection is solely contributed by spontaneous RNA dissociation (full-length and 5' cleavage fragments) from the activator strands.

The RNA dissociation rates were obtained through model fitting for each construct under different reaction condition (Figure 3.6B). The measured spontaneous RNA dissociation rates (reaction condition (i)) ranged from 0.05 to 0.18 min⁻¹. The presence of theophylline has little nonspecific effect on the observed dissociation rates by examining the rates obtained for the sTRSV construct in the absence (1.66 min⁻¹) and presence (1.54 min⁻¹) of 5 mM theophylline. The observed RNA dissociation rates obtained for L2b8 (0.13, 0.09 min⁻¹) and L2b8-a1 (0.55, 0.17 min⁻¹) in the absence and presence of 5 mM theophylline, respectively, were generally in close agreement with those obtained through the trans-blocking gel-based assays (Figure 3.4B). However, the measured RNA dissociation rate (0.09 min⁻¹) for the L2b8 construct in the presence of theophylline was significantly greater than the corresponding gel-based cleavage rate (0.025 min⁻¹) obtained from the trans-blocking strategy, and was comparable to the spontaneous RNA dissociation rate (0.05 min⁻¹) measured in the absence of MgCl₂. This result suggests that our current SPR-based assay is limited by the spontaneous dissociation of RNA from the sensor surface, and thus may not be applicable to characterize ribozyme constructs that exhibit slow cleavage rates.

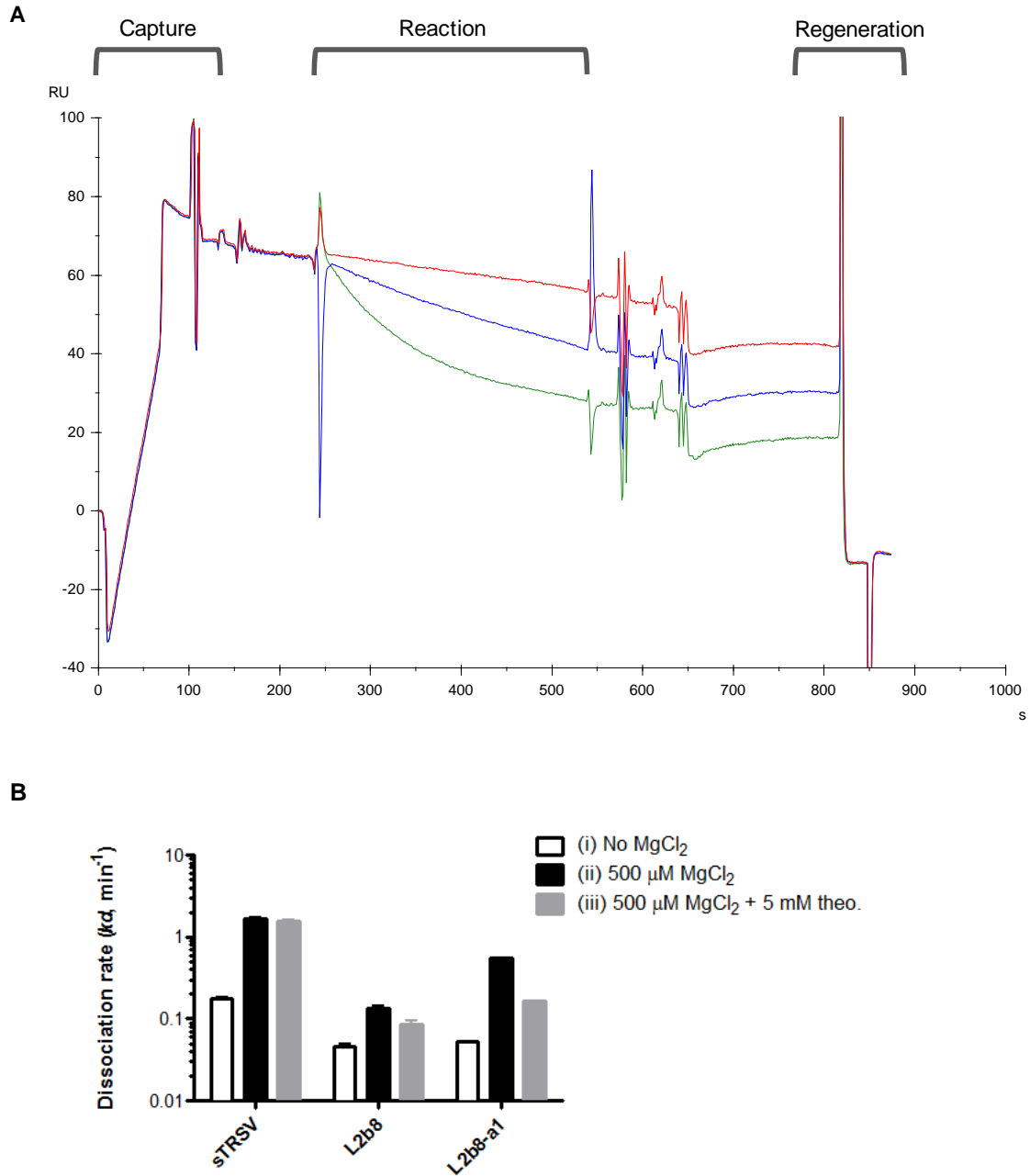


Figure 3.6 The observed RNA dissociation rate are closely correlated to the corresponding cleavage rates. (A) The SPR-based assays were performed on the cis-blocked sTRSV, L2b8, and L2b8-a1 constructs. The reactions were initiated by injecting buffers ($500 \mu\text{M MgCl}_2$, 100 mM NaCl , and 50 mM Tris-HCl (pH 7.0)) containing: (i) no MgCl_2 ; (ii) $500 \mu\text{M MgCl}_2$; and (iii) $500 \mu\text{M MgCl}_2$ and $5 \text{ mM theophylline}$. A representative sensorgram for the characterization of the L2b8-a1 construct at three different assay conditions is shown here. The detailed assay steps are indicated. (B) The injection portions of the sensorgrams were fit to a first-order decay equation to obtain the RNA dissociation rate constants (k_d) (Supplementary Figure S3.5). RNA dissociation rate

constants and errors are reported as the mean and standard deviation from at least three independent assays.

3.3 DISCUSSION

We described a ribozyme-blocking strategy to support efficient generation of full-length RNA transcripts containing ribozyme constructs through *in vitro* transcription reactions. In contrast to the traditional trans-blocking strategy that requires laborious PAGE purification process for the recovery of full-length transcription products, our cis-blocking strategy offers a rapid two-step process (transcription and activation) to yield large quantities of full-length RNA. We demonstrated the cis-blocking strategy on a variety of different ribozyme elements, including natural ribozymes and synthetic ribozyme devices. The cleavage rate constants associated with the full-length RNA generated from the cis- and trans- blocking strategies were shown to be in close agreement and correlate with one another, thus supporting our cis-blocking strategy as an efficient method for ribozyme characterization.

We employed a robust toehold-mediated strand-displacement reaction to facilitate the activation of RNA. A similar toehold-mediated activation mechanism has been applied to the kinetic study of the hepatitis delta virus (HDV) ribozyme through the use of antisense oligomers that target the upstream natural cis-blocking sequence (19). We rationally designed the blocking, activation, and stabilizing sequences to achieve an optimal blocking efficiency up to ~90% for the sTRSV ribozyme. Previous kinetic studies on the sTRSV ribozyme have shown that ~50% of the full-length RNA generated by the trans-blocking strategy remained uncleaved at the end of reaction (9). In contrast, the full-length RNA generated by our cis-blocking strategy resulted in only ~16%

uncleaved products at the end of reaction, suggesting that full-length RNA prepared by our method is less prone to misfolding.

Our cis-blocking strategy utilizes a trans-acting DNA strand to activate the blocked RNA, allowing the development of an 'on-chip' activation strategy by generating a reaction surface immobilized with DNA activator strands. We developed a rapid, label-free cleavage assay based on SPR, which allows real-time monitoring of ribozyme cleavage. Our SPR-based assay offers several unique advantages over the more traditional gel-based assay in that: (i) it requires no radioactivity; (ii) it requires little material (microfluidics-based flow system); and (iii) it is highly automatable. However, to broaden the utility of our SPR-based strategy for the quantification of ribozyme cleavage rates, efforts need to be made to address several immediate challenges. Our strategy is currently based on a capture-based sensor surface. Although such strategy allows the reuse of the surface by regeneration, the measured observed RNA dissociation rate is contributed to both cleavage-dependent (3' cleaved fragments) and spontaneous (full-length and 5' cleaved fragments) dissociation rates. Thus, the spontaneous RNA dissociation rate prevents the quantitative measurement of cleavage rates solely based on the SPR-based assays. In addition, our current SPR-based assay is limited by the maximum injection volume allowed for the given instrument, which presents a challenge for the characterization of ribozyme constructs exhibiting low cleavage activities (thus requiring a longer injection).

To allow direct measurement of cleavage rates through the SPR-based assays, efforts can be directed toward enhancing the stability of the hybridization reaction between the RNA and the DNA activator strand by extending the length of the RNA

activation sequence through its 5' end. Further optimization of the blocking and stabilizing sequences may be necessary to ensure that a longer activation sequence does not interact nonspecifically with neighboring sequences, thus impacting the blocking efficiency. Alternative activator backbone, such as peptide nucleic acid (PNA), may also be considered to enhance the stability of the RNA-captured sensor surface, as the PNA-RNA duplex has been shown to exhibit greater thermal stability than the corresponding PNA-DNA and DNA-DNA duplexes (20). To expand the range of cleavage activities that can be analyzed by the SPR-based assays, strategies that allow a longer reaction have been described by either directly using the characterization buffer as the instrument running buffer (thus requiring no injection of the characterization buffer) or modifying the SPR instrument with an external peristaltic pump (21). With further development and optimization, the SPR-based cleavage assay will offer a powerful strategy for rapidly quantifying cleavage rates for a wide variety of ribozyme constructs, thereby supporting the functional design of RNA for diverse applications.

3.4 MATERIALS AND METHODS

3.4.1 Preparation of DNA templates for T7 transcription reaction

DNA synthesis was performed by Integrated DNA Technologies (Coralville, IA) or the Protein and Nucleic Acid Facility (Stanford, CA). PCR products were used as DNA templates for *in vitro* T7 transcription reaction. For the cis-blocking strategy, PCR products were amplified from templates using forward primer T7-fwd (5'-TTCTAATACGACTCACTATAGG) and corresponding reverse primers that are specific to each construct (Supplementary Table S3.1), respectively.

3.4.2 Generation of full-length RNA through cis-blocking strategy

A total of 1-2 μg of PCR product was transcribed in a 25 μl reaction, consisting of the following components: 1 \times RNA Pol Reaction Buffer (New England Biolabs, Ipswich, MA), 2.5 mM of each rNTP, 1 μl RNaseOUT (Invitrogen, Carlsbad, CA), 10 mM MgCl_2 , 1 μl T7 Polymerase (New England Biolabs), and 0.5 μCi α - ^{32}P -GTP (MP Biomedicals, Solon, OH). After incubation at 37°C for 2 hr, NucAway Spin Columns (Ambion, Austin, TX) were used to remove unincorporated nucleotides from the transcription reactions according to manufacturer's instructions. The transcription products were purified with the RNA Clean & ConcentratorTM-5 (Zymo Research, Irvine, CA) kit according to manufacturer's instructions.

3.4.3 Gel-based ribozyme cleavage assays

All gel-based ribozyme cleavage assays were performed in a physiologically-relevant reaction buffer composed of 500 μM MgCl_2 , 100 mM NaCl, and 50 mM Tris-HCl (pH 7.0) at 37°C. Full-length RNA generated from the cis-blocking strategy were first incubated with 60 pmol DNA activator strand (5'- AAACAAC TTTGTTTGTTC CCC) for 2 min to activate the blocked RNA. Full-length RNA generated from the trans-blocking strategy were incubated at 95°C for 5 min, cooled at a rate of -1.3°C to 37°C, and held there for 10 min to allow equilibration of secondary structure. A zero time-point aliquot was taken prior to initiating the self-cleavage reaction with the addition of MgCl_2 . Reactions were quenched at specified time points with addition of 3 volumes of RNA stop/load buffer (95% formamide, 30 mM EDTA, 0.25% bromophenol blue, 0.25% xylene cyanol) on ice. Samples were heated to 95°C for 5 min, snap cooled on ice for 5

min, and size-fractionated on a denaturing (8.3 M Urea) 10% polyacrylamide gel at 25 W for 45 to 60 min. Gels were exposed overnight on a phosphor screen and imaged on a FX Molecular Imager (Bio-Rad, Hercules, CA). The relative levels of the full-length transcript and cleaved products were determined by phosphorimaging analysis. The cleaved product fraction at each time point (F_t) was fit to the single exponential equation $F_t = F_0 + (F_\infty - F_0) \times (1 - e^{-kt})$ using Prism 5 (GraphPad), where F_0 and F_∞ are the fractions cleaved before the start of the reaction and at the reaction endpoint, respectively, and k is the first-order rate constant of self-cleavage. All reported cleavage rates are the mean of at least three independent experiments.

3.4.4 Biacore sensor chip surface generation

Biosensor experiments were performed on a Biacore X100 instrument (Biacore, Uppsala, Sweden). A CM5 sensor chip (Biacore) was docked in the Biacore X100 and equilibrated with HBS-N buffer at 25°C. The DNA activator strand (5'-AAACAAC TTTGTTTGT TTTCCCCC-/AmMO/), with an amino modification on its 3' end, was immobilized to the chip surface via standard amine-coupling chemistry. Briefly, the carboxymethyl surface of the CM5 chip was activated for 7 min at a flow rate of 5 μ l/min using a 1:1 volume ratio of 0.4 M 1-ethyl-3-(3-dimethylaminopropyl) carbodiimide (Biacore) and 0.1 M N-hydroxysuccinimide (Biacore). A molar ratio of 1:60 of DNA activator to cetyl trimethylammonium bromide (Amresco, Solon, OH) was diluted in 10 mM HEPES buffer (Sigma, St. Louis, MO) to a final concentration of 10 μ M and 0.6 mM, respectively, and injected over the activated surface for 10 min at a flow rate of 5 μ l/min. Excess activated groups were blocked by an injection of 1 M

ethanolamine (Biacore), pH 8.5, for 7 min at a flow rate of 5 $\mu\text{l}/\text{min}$. The immobilization reaction was performed on both flow cells (FC1, FC2), where FC1 was used as a reference cell to correct for bulk refractive index changes, matrix effects, nonspecific binding, injection noise and baseline drift (22). Approximately 1600 RU of the activator strand was immobilized using this protocol.

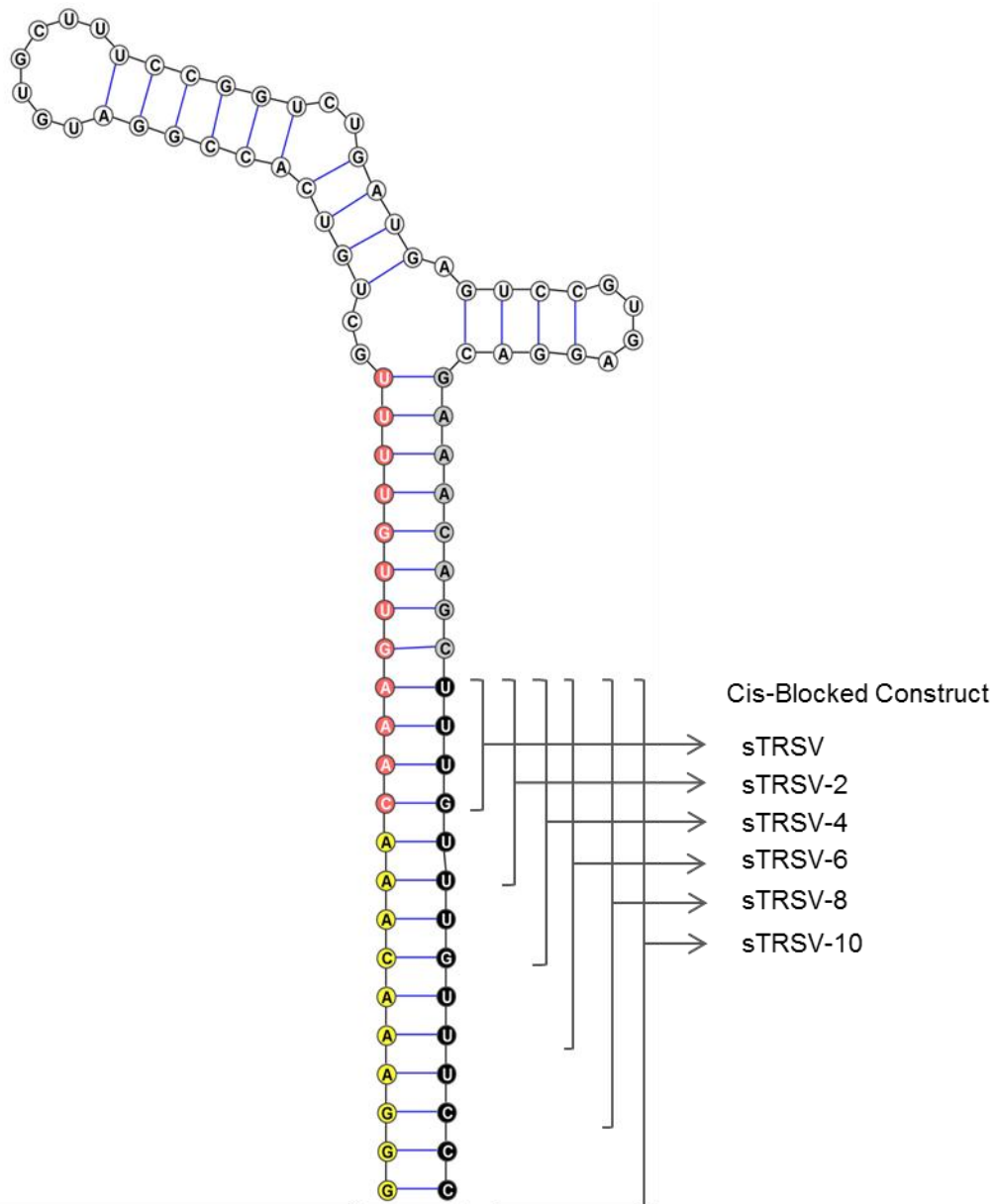
3.4.5 Label-free SPR-based ribozyme cleavage assays

Full-length RNA was prepared by the cis-blocking strategy without the radiolabelled nucleotides. The Biacore X100 instrument was equilibrated with the physiologically-relevant reaction buffer at 37°C prior to all ribozyme cleavage assays. The SPR baseline was stabilized by performing 2-5 startup cycles, each cycle includes a capture and a regeneration step. The capture step was performed by an injection of a total of 10-25 ng transcribed RNA diluted in the reaction buffer over the reaction flow cell (FC2) for 1 min at a flow rate of 10 $\mu\text{l}/\text{min}$. The capture step typically yielded ~50-300 RU of the SPR signal for the described constructs. The regeneration step was performed by an injection of 25 mM NaOH over both flow cells for 30 sec at a flow rate of 30 $\mu\text{l}/\text{min}$.

Following the startup cycles, assay cycles were performed. Each assay cycle includes a capture, a reaction, and a regeneration step. The capture and regeneration steps were performed the same as those in the startup cycle. The reaction step was performed by an injection of the running buffer or running buffers containing 500 μM MgCl_2 with or without 5 mM theophylline over both FCs for 5 min at a flow rate of 10 $\mu\text{l}/\text{min}$. Biacore sensorgram processing and analysis were performed using Biacore X100 Evaluation

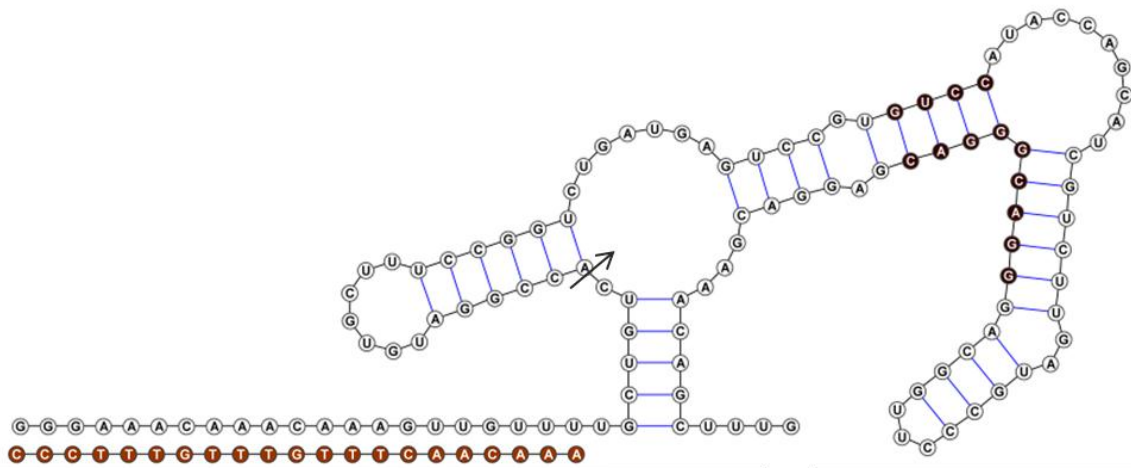
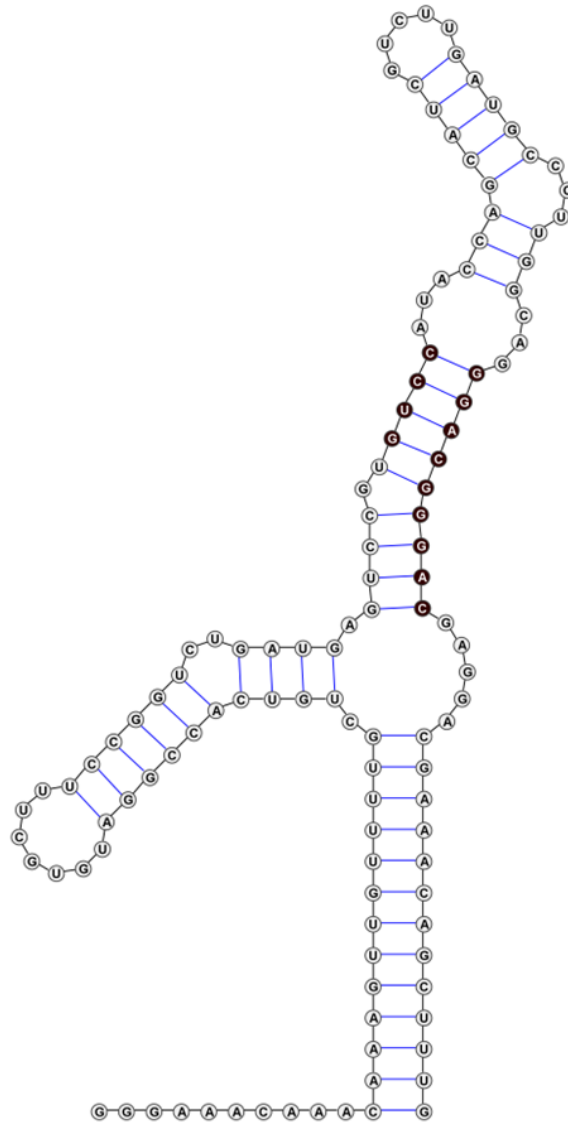
Software v2.0 (Biacore). Due to the slight time delay at which injected analyte reaches the respective flow cells, the resultant sharp spikes at the beginning and the end of injection were excluded from the analysis (23). The processed sensorgram (R) was fit to a simple exponential equation $R = R_0 \times (e^{-kd t} - 1) + \text{offset}$, where R_0 (fit globally for a given replicate) is the initial SPR signal before the cleavage reaction, offset (fit locally for a given replicate) is the residual response at the end of the cleavage reaction, and kd is the first-order RNA dissociation rate constant. Reported values are the mean of at least three independent experiments.

3.5 Supplementary Information

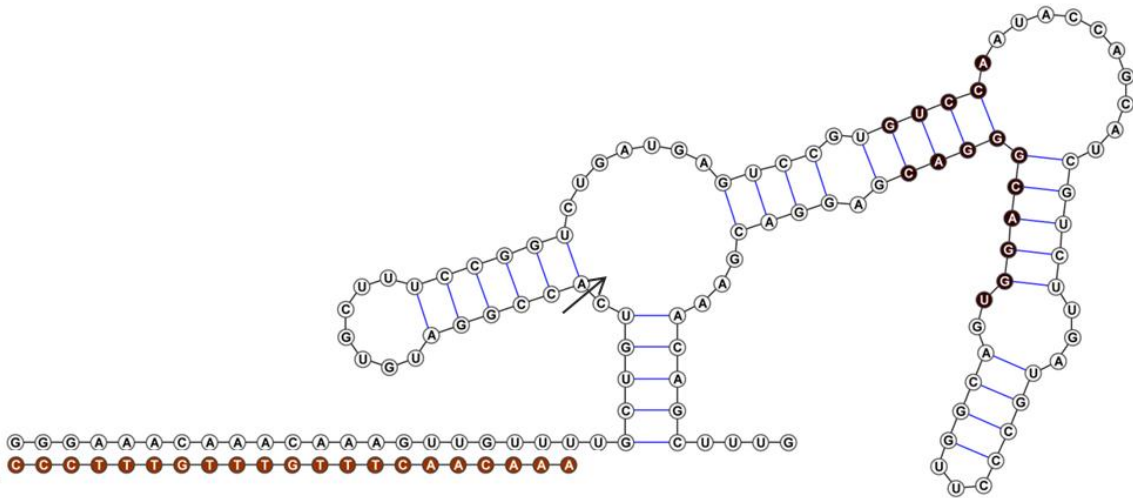
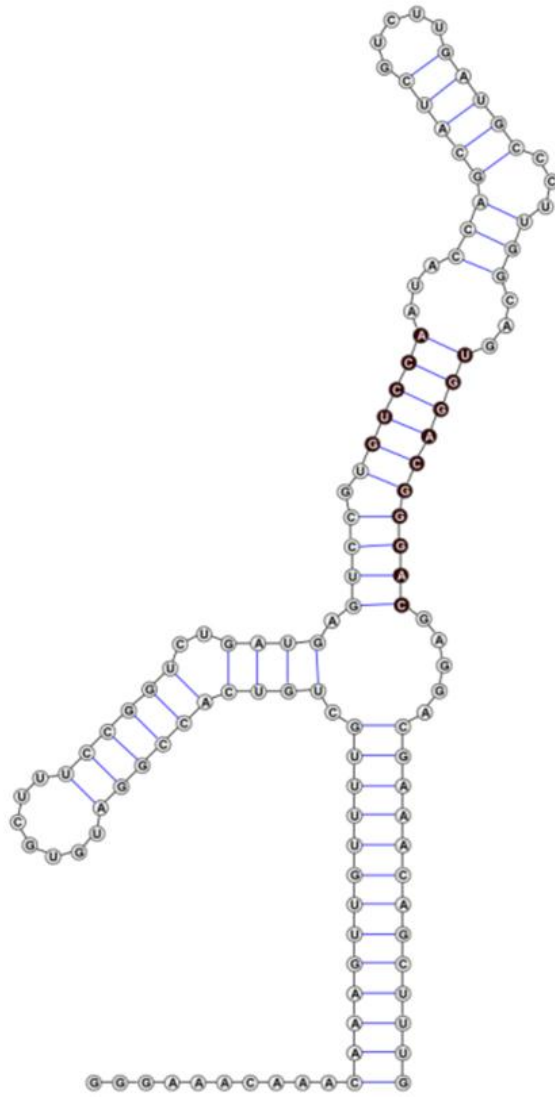


Supplementary Figure S3.1 Cis-blocked sTRSV constructs with varying stabilizing sequence length. The stabilizing sequence in the cis-blocked sTRSV construct (Figure 3.2) is increased in 2 nt increment to generate sTRSV-2, -4, -6, -8, and -10 constructs (Supplementary Table S3.1). The targeted ribozyme sequence, and the RNA blocking, activation, and stabilizing sequences are indicated in grey, red, yellow, and black, respectively. The additional 2, 4, 6, 8, and 10 nt to the stabilizing sequence in the original cis-blocked sTRSV construct results in a toehold length of 8, 6, 4, 2, and 0 nt, respectively.

B L2b1

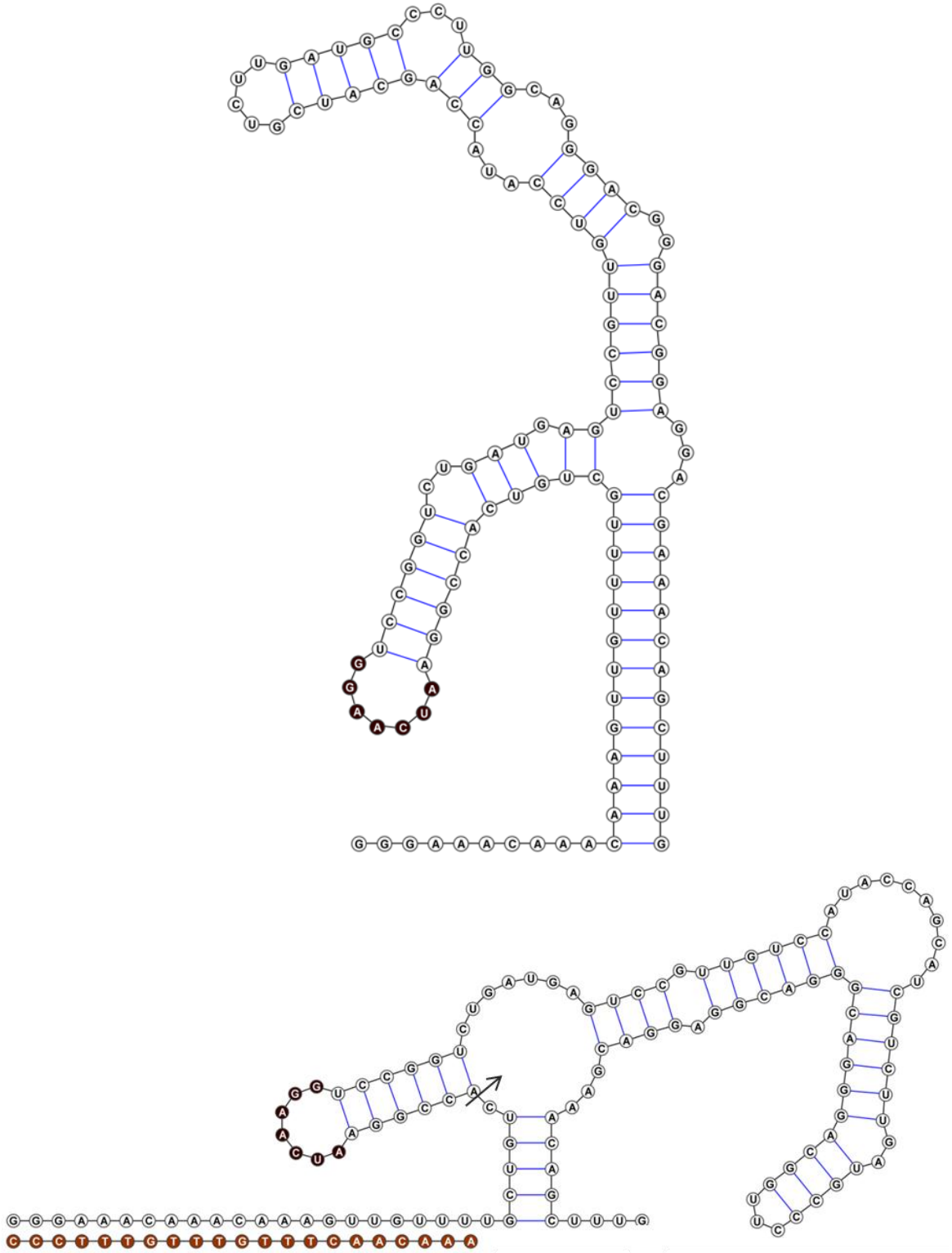


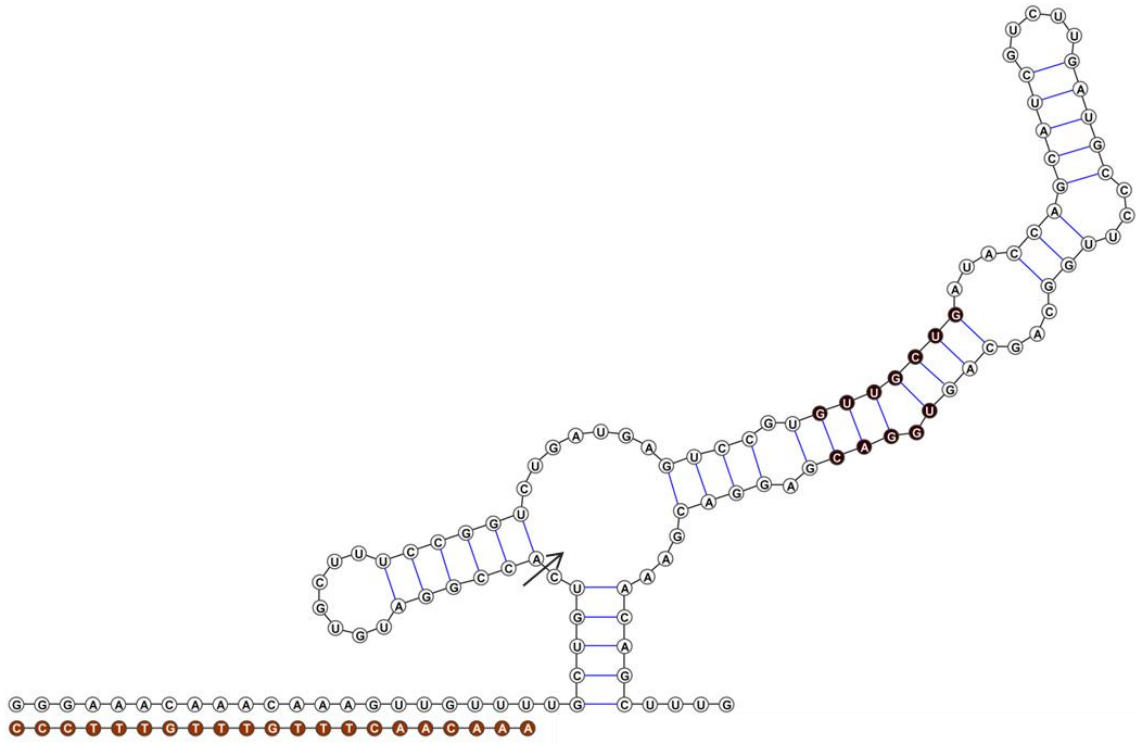
C L2b5



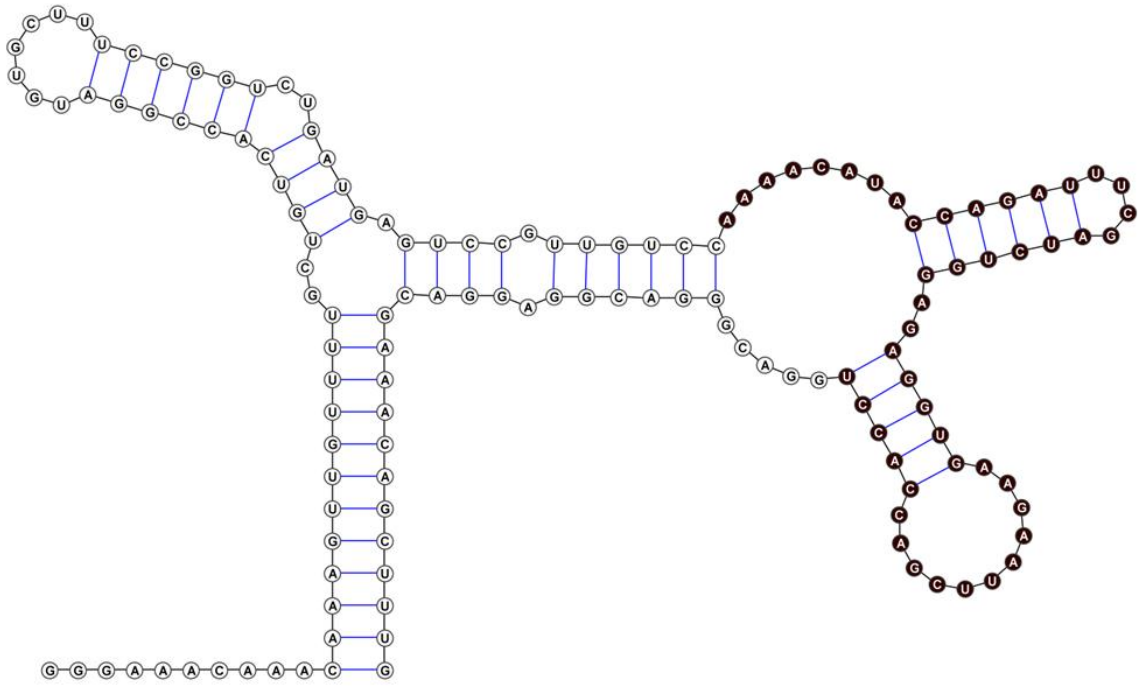
G-G-G-A-A-A-C-A-A-A-C-A-A-G-U-U-G-U-U-U-G-C-U-U-U-G
C-C-T-T-T-G-T-T-C-A-A-C-A-A

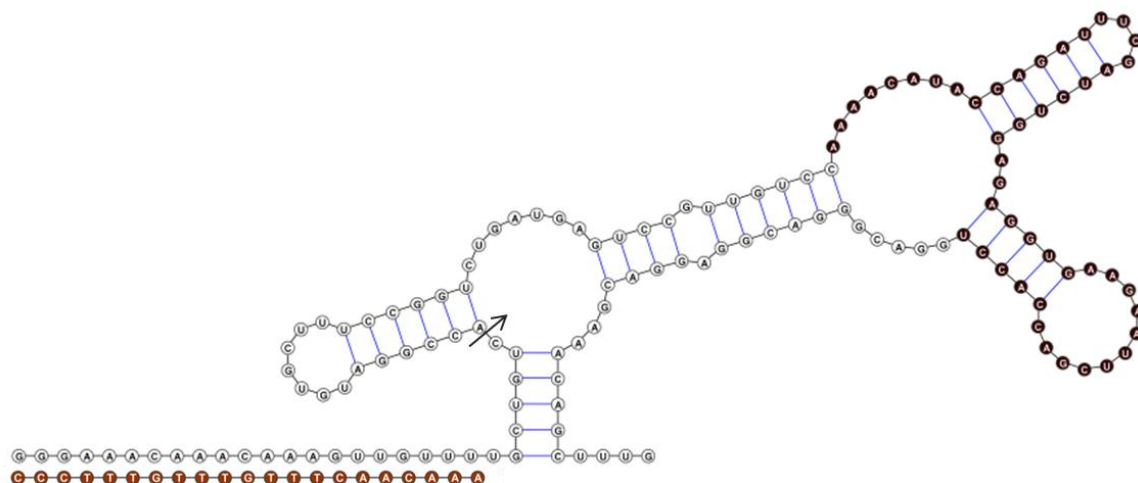
D L2b8-a1





F L2b8tc



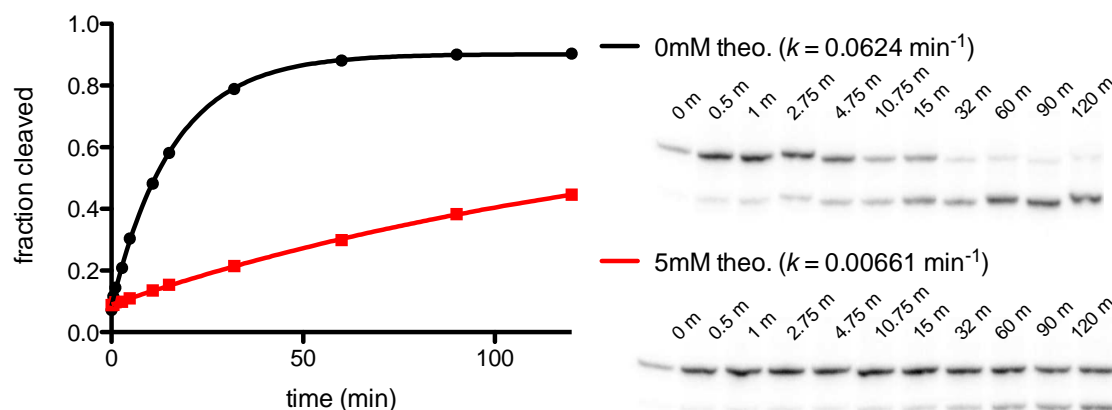


Supplementary Figure S3.2 Cis-blocked constructs for synthetic ribozyme devices composed of different functional RNA components. The same blocking (targeting the same sTRSV ribozyme sequence), activation, and stabilizing sequences shown in Figure 2 were directly incorporated into the synthetic ribozyme devices to generate the corresponding cis-blocked ribozyme constructs (Supplementary Table S3.1). The targeted ribozyme sequence, RNA blocking, activation, stabilizing sequences, and DNA activator are indicated in grey, red, yellow, black, and brown, respectively, for the (A) L2b8 construct. The sensor (RNA aptamer), transmitter, and actuator (sTRSV ribozyme) in the L2b8 construct are indicated in green, blue, and white, respectively. For the subsequent constructs, only components that are different from those in the L2b8 device are indicated in brown. The blocked (top) and activated (bottom) conformations are shown for each construct. The (A) L2b8, (B) L2b1, and (C) L2b5 devices are theophylline-responsive ribozyme ON devices that differ slightly in the transmitter sequences. The (D) L2b8-a1 device was modified from the L2b8 device by incorporating a ribozyme variant that exhibits improved cleavage activity (see Chapter 2). The (E) L2bOFF1 device is a theophylline-responsive ribozyme OFF device that is composed of a transmitter sequence that is different from those in the ribozyme ON devices. The (F) L2b8tc device is a tetracycline-responsive ribozyme ON device that was generated by directly replacing the theophylline aptamer in the L2b8 device with the tetracycline aptamer (see Chapter 2). Secondary structures were predicted by RNAstructure folding software (16) and rendered using VARNA software (8).

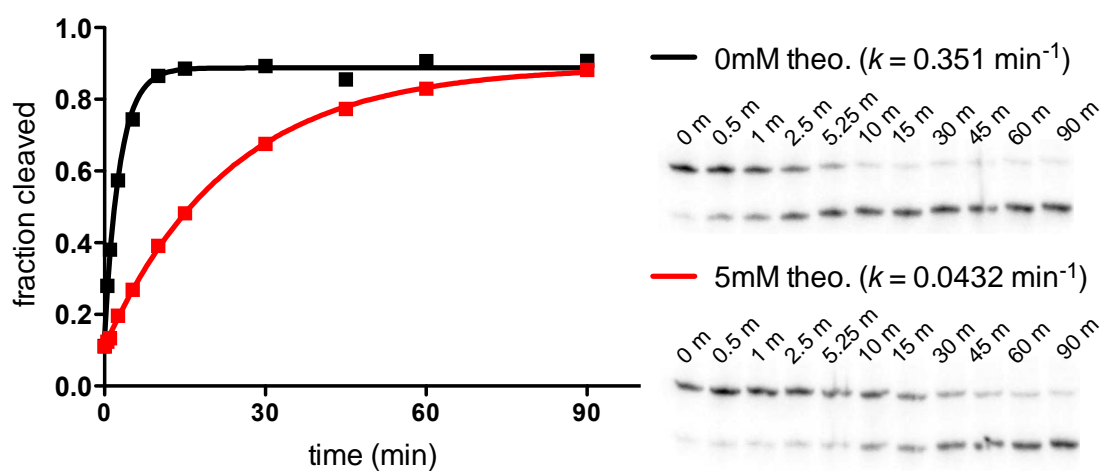


Supplementary Figure S3.3 Gel analysis of the transcription products for the L2b8 construct without the cis-blocking sequence. PCR products, which were used as DNA templates for *in vitro* T7 transcription reactions, were amplified using forward and reverse primers T7-L1-2-fwd (5'- TTCTAATACGACTCACTATAGGGACCTAGGAA ACAAACAAAGCTGTCACC) and L1-2-rev (5'-GGCTCGAGTTTTTATTTTTCTTTT TGCTGTTTCG), respectively. The transcription reactions were performed in the absence and presence of 5 mM theophylline at the same reaction conditions as described for the generation of cis-blocked RNA (see Materials and Methods). A previously described non-switch control, L2Theo (3), which lacks the transmitter sequence in the L2b8 device (thus only adopting the ribozyme-inactive conformation and cleaves) was transcribed, resulting in 5' (25 nt) and 3' (109 nt) cleaved fragments. In addition, a ribozyme-inactive control, L2Theo Contl, generated by randomizing the ribozyme catalytic core in the L2Theo construct (thus abolishing the ribozyme cleavage activity) was transcribed, resulting in a full-length fragment (134 nt). The transcription products were size-fractionated on a denaturing (7 M urea) 10% polyacrylamide gel at 25 W for 45 min and imaged by phosphorimaging analysis. The transcription of the L2b8 construct without the cis-blocking sequence resulted in 5' (25 nt) and 3' (116 nt) cleavage fragments, and little full-length (141 nt) fragment was observed.

A L2b8:



B L2b8-a1:



C

RNA Device	Cleavage Rate (k , min^{-1})	
	0 mM theophylline	5 mM theophylline
L2b8	0.063 ± 0.001	0.008 ± 0.002
L2b8-a1	0.351 ± 0.007	0.043 ± 0.007

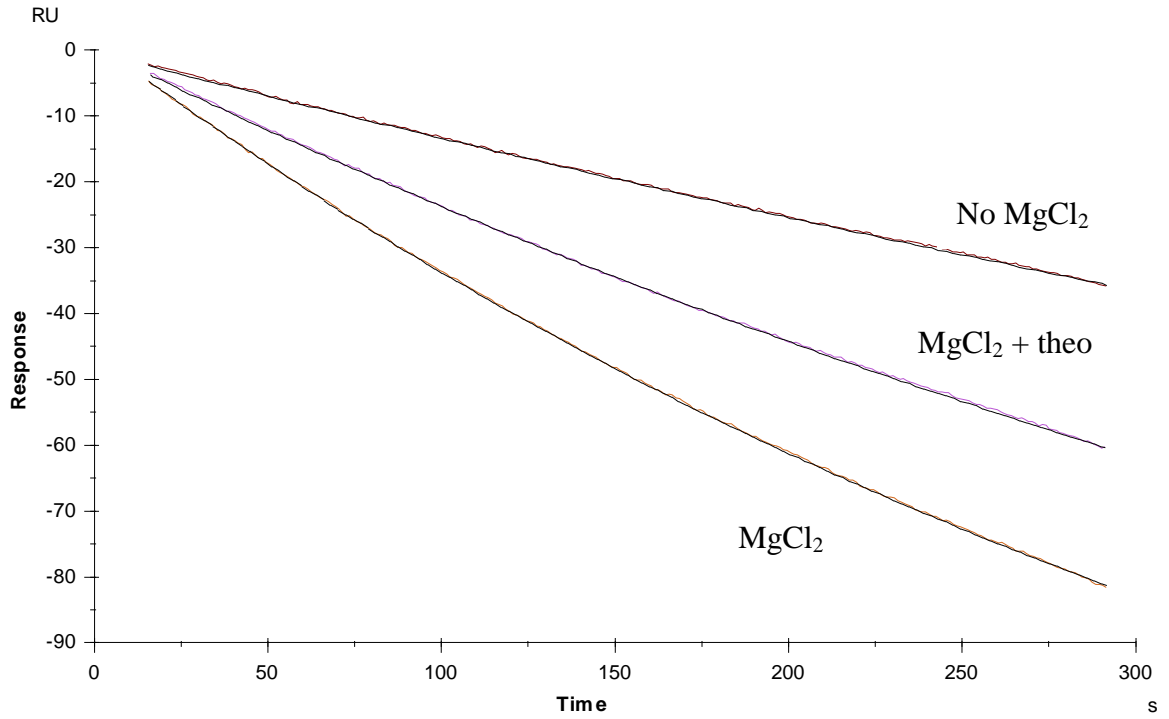
Supplementary Figure S3.4 Representative gel-based cleavage assays for measuring cleavage rate constants (k) for RNA generated from the cis-blocking strategy. A representative assay is shown for each cis-blocked construct in the absence and presence (0 and 5 mM, respectively) of theophylline: (A) L2b8 and (B) L2b8-a1. Bands for the full-length uncleaved substrate (UC) and longer cleaved product (3'C) are shown, the shorter 5'C product is omitted from the inset image for clarity. Methods used to prepare

full-length, uncleaved RNA transcripts and conditions of the cleavage assays are detailed in the Materials and Methods section of the main text. Briefly, cis-blocked RNA was incubated with the DNA activator in a buffer (100 mM NaCl, 50 mM Tris-HCl (pH 7.0)) for 2 min to activate the blocked RNA. A zero time point aliquot was removed prior to initiating the reaction with addition of MgCl₂ to a final concentration of 500 μM. Reactions were quenched at the indicated time points. Phosphorimaging analysis of relative levels of the UC, 5'C, and 3'C bands was used to determine the fraction cleaved at each time point (F_t). The fraction cleaved at the beginning (F_0) and end of reaction (F_∞) varied between assays, but all assays were well-fit to the single exponential equation ($R^2 > 0.95$):

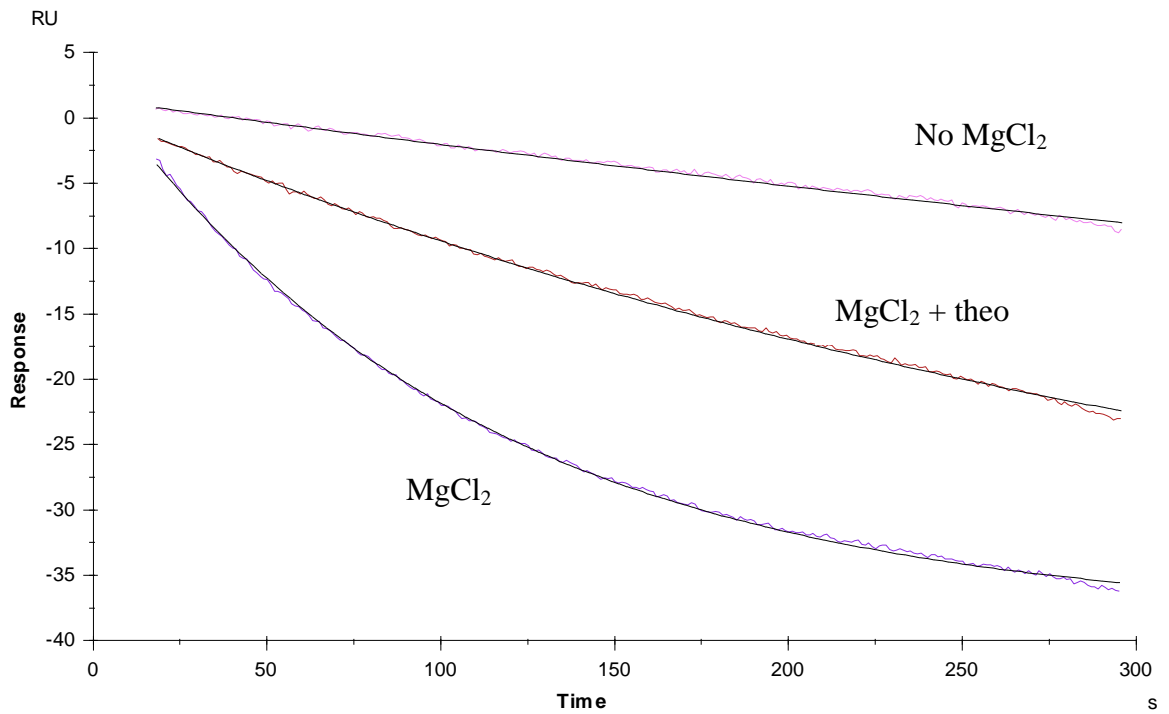
$$F_t = F_0 + (F_\infty - F_0) \times (1 - e^{-kt})$$

The black and red fit lines represent assays performed at 0 and 5 mM theophylline, respectively. (C) The cleavage rate constant value (k) was determined for each assay. The reported k for each device and theophylline assay condition is the mean and standard deviation of at least three independent experiments.

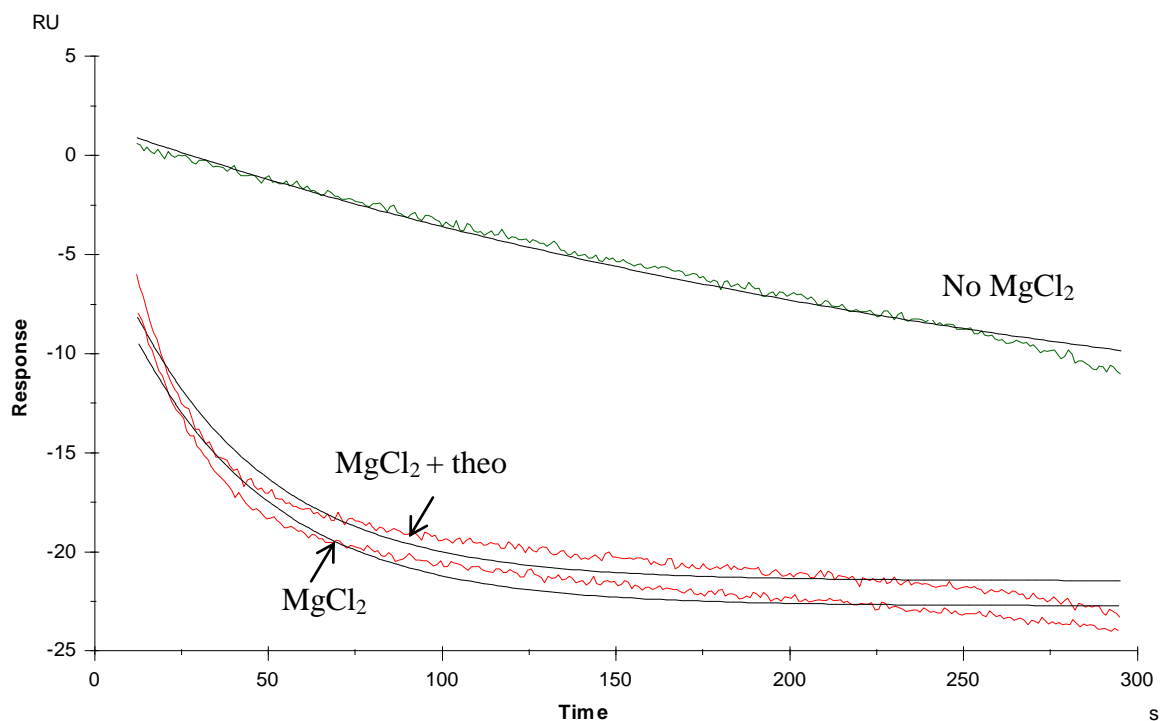
A L2b8 (χ^2 : 0.0255):



B L2b8-a1 (χ^2 : 0.0395):



C sTRSV(Chi^2 : 0.33):



D

RNA Device	Dissociation Rate (k , min^{-1})		
	No MgCl ₂	MgCl ₂	MgCl ₂ + theo
L2b8	0.047 ± 0.003	0.133 ± 0.011	0.087 ± 0.008
L2b8-a1	0.052 ± 0.001	0.552 ± 0.006	0.166 ± 0.001
sTRSV ribozyme	0.18 ± 0.01	1.66 ± 0.04	1.54 ± 0.10

Supplementary Figure S3.5 Representative SPR-based cleavage assays for measuring RNA dissociation rate constants (kd) for RNA generated from the cis-blocking strategy. A representative Biacore sensorgram is shown for each cis-blocked construct: (A) L2b8, (B) L2b8-a1, (C) sTRSV. The assays were performed in reactions buffers (100 mM NaCl, 50 mM Tris-HCl (pH 7.0)) containing: (i) no MgCl₂; (ii) 500 μM MgCl₂; and (iii) 500 μM MgCl₂ and 5 mM theophylline at 37°C. The capture, reaction, and regeneration steps in the assay cycle are indicated for the L2b8 sensorgrams. Methods used to prepare full-length RNA transcripts and conditions of the cleavage assays are detailed in the Materials and Methods section of the main text. The reaction step of the sensorgram was well-fit to the single exponential equation ($\text{Chi}^2 < 0.34$):

$$R_t = R_0 \times (e^{-kd} - 1) + \text{offset}$$

(D) The RNA dissociation rate (kd) was determined for each assay. The reported kd for each construct are the mean and standard deviation of at least three independent experiments.

Supplementary Table S3.1 Sequences of primers and templates for all described cis-blocked constructs in this work. The T7 promoter region in the template sequence is indicated in bold.

Primer	Sequence
T7-fwd	TTCTAATACGACTCACTATAGG
sTRSV-rev	CAAAGCTGTTTCGTCCTCAC
sTRSV-2-rev	AACAAAGCTGTTTCGTCCTCAC
sTRSV-4-rev	CAAACAAAGCTGTTTCGTCCTCAC
sTRSV-6-rev	AACAAACAAAGCTGTTTCGTCCTCAC
sTRSV-8-rev	GAAACAAACAAAGCTGTTTCGTCCTCAC
sTRSV-10-rev	GGGAAACAAACAAAGCTGTTTCGTCCTCAC
L2b1-rev	CAAAGCTGTTTCGTCCTCGTCCCGTCC
L2b5-rev	Same as b-L2b1-rev
L2b8-rev	CAAAGCTGTTTCGTCCTCCGT
L2b8-a1-rev	Same as b-L2b8-rev
L2bOFF1-rev	CAAAGCTGTTTCGTCCTCGTCCACTGC
L2b8tc-rev	Same as b-L2b8-rev
Template	Sequence
sTRSV	TTCTAATACGACTCACTATAGG GAAACAAACAAAGTTGTT TTGCTGTCACCGGATGTGCTTTCCGGTCTGATGAGTCCGTGA GGACGAAACAGCTTTG
sTRSV-2	TTCTAATACGACTCACTATAGG GAAACAAACAAAGTTGTT TTGCTGTCACCGGATGTGCTTTCCGGTCTGATGAGTCCGTGA GGACGAAACAGCTTTGTT
sTRSV-4	TTCTAATACGACTCACTATAGG GAAACAAACAAAGTTGTT TTGCTGTCACCGGATGTGCTTTCCGGTCTGATGAGTCCGTGA GGACGAAACAGCTTTGTTG
sTRSV-6	TTCTAATACGACTCACTATAGG GAAACAAACAAAGTTGTT TTGCTGTCACCGGATGTGCTTTCCGGTCTGATGAGTCCGTGA GGACGAAACAGCTTTGTTT
sTRSV-8	TTCTAATACGACTCACTATAGG GAAACAAACAAAGTTGTT TTGCTGTCACCGGATGTGCTTTCCGGTCTGATGAGTCCGTGA GGACGAAACAGCTTTGTTT
sTRSV-10	TTCTAATACGACTCACTATAGG GAAACAAACAAAGTTGTT TTGCTGTCACCGGATGTGCTTTCCGGTCTGATGAGTCCGTGA GGACGAAACAGCTTTGTTT
L2b1	TTCTAATACGACTCACTATAGG GAAACAAACAAAGTTGTT TTGCTGTCACCGGATGTGCTTTCCGGTCTGATGAGTCCGTGT CCATACCAGCATCGTCTTGATGCCCTTGGCAGGGACGGGAC GAGGACGAAACAGCTTTG
L2b5	TTCTAATACGACTCACTATAGG GAAACAAACAAAGTTGTT

TTGCTGTCACCGGATGTGCTTCCGGTCTGATGAGTCCGTGT
 CCAATACCAGCATCGTCTTGATGCCCTTGGCAGTGGACGGG
 ACGAGGACGAAACAGCTTTG
 L2b8 **TTCTAATACGACTCACTATAGGGAAACAAACAAAGTTGTT**
 TTGCTGTCACCGGATGTGCTTCCGGTCTGATGAGTCCGTTG
 TCCATACCAGCATCGTCTTGATGCCCTTGGCAGGGACGGGA
 CGGAGGACGAAACAGCTTTG
 L2b8-a1 **TTCTAATACGACTCACTATAGGGAAACAAACAAAGTTGTT**
 TTGCTGTCACCGGAATCAAGGTCCGGTCTGATGAGTCCGTT
 GTCCATACCAGCATCGTCTTGATGCCCTTGGCAGGGACGGG
 ACGGAGGACGAAACAGCTTTG
 L2bOFF1 **TTCTAATACGACTCACTATAGGGAAACAAACAAAGTTGTT**
 TTGCTGTCACCGGATGTGCTTCCGGTCTGATGAGTCCGTGT
 TGCTGATACCAGCATCGTCTTGATGCCCTTGGCAGCAGTGG
 ACGAGGACGAAACAGCTTTG
 L2b8tc **TTCTAATACGACTCACTATAGGGAAACAAACAAAGTTGTT**
 TTGCTGTCACCGGATGTGCTTCCGGTCTGATGAGTCCGTTG
 TCCAAAACATACCAGATTCGATCTGGAGAGGTGAAGAATT
 CGACCACCTGGACGGGACGGAGGACGAAACAGCTTTG

Acknowledgements

We thank J Schuman of GE and M Eckhart of the Stanford PAN facility. This work was supported by the National Institutes of Health (R01GM086663), the National Science Foundation (CBET-0917638, CCF-0943269), the Defense Advanced Research Projects Agency (HR0011-11-2-0002), and the National Sciences and Engineering Research Council of Canada (fellowship to ABK).

Contributions

JCL designed research, performed research, and wrote the paper; ABK designed and performed research associated with the *in vitro* characterization of ribozyme cleavage rates and wrote the paper; CDS designed research and wrote the paper.

References

1. Nandagopal, N. and Elowitz, M.B. (2011) Synthetic biology: integrated gene circuits. *Science*, **333**, 1244-1248.
2. Liang, J.C., Bloom, R.J. and Smolke, C.D. (2011) Engineering biological systems with synthetic RNA molecules. *Mol Cell*, **43**, 915-926.
3. Win, M.N. and Smolke, C.D. (2007) A modular and extensible RNA-based gene-regulatory platform for engineering cellular function. *Proceedings of the National Academy of Sciences*, **104**, 14283-14288.
4. Chen, Y.Y., Jensen, M.C. and Smolke, C.D. (2010) Genetic control of mammalian T-cell proliferation with synthetic RNA regulatory systems. *Proc Natl Acad Sci U S A*, **107**, 8531-8536.
5. Wieland, M. and Hartig, J.S. (2008) Improved aptazyme design and in vivo screening enable riboswitching in bacteria. *Angew Chem Int Ed Engl*, **47**, 2604-2607.
6. Win, M.N. and Smolke, C.D. (2008) Higher-order cellular information processing with synthetic RNA devices. *Science*, **322**, 456-460.
7. Beisel, C.L. and Smolke, C.D. (2009) Design principles for riboswitch function. *PLoS Comput Biol*, **5**, e1000363.
8. Darty, K., Denise, A. and Ponty, Y. (2009) VARNA: Interactive drawing and editing of the RNA secondary structure. *Bioinformatics*, **25**, 1974-1975.
9. Nelson, J.A., Shepotinovskaya, I. and Uhlenbeck, O.C. (2005) Hammerheads derived from sTRSV show enhanced cleavage and ligation rate constants. *Biochemistry*, **44**, 14577-14585.

10. Mercure, S., Lafontaine, D., Ananvoranich, S. and Perreault, J.P. (1998) Kinetic analysis of delta ribozyme cleavage. *Biochemistry*, **37**, 16975-16982.
11. Stage-Zimmermann, T.K. and Uhlenbeck, O.C. (1998) Hammerhead ribozyme kinetics. *RNA*, **4**, 875-889.
12. Khvorova, A., Lescoute, A., Westhof, E. and Jayasena, S.D. (2003) Sequence elements outside the hammerhead ribozyme catalytic core enable intracellular activity. *Nat Struct Biol*, **10**, 708-712.
13. Singh, K.K., Parwaresch, R. and Krupp, G. (1999) Rapid kinetic characterization of hammerhead ribozymes by real-time monitoring of fluorescence resonance energy transfer (FRET). *RNA*, **5**, 1348-1356.
14. Penedo, J.C., Wilson, T.J., Jayasena, S.D., Khvorova, A. and Lilley, D.M. (2004) Folding of the natural hammerhead ribozyme is enhanced by interaction of auxiliary elements. *RNA*, **10**, 880-888.
15. Rich, R.L., Papalia, G.A., Flynn, P.J., Furneisen, J., Quinn, J., Klein, J.S., Katsamba, P.S., Waddell, M.B., Scott, M., Thompson, J. *et al.* (2009) A global benchmark study using affinity-based biosensors. *Anal Biochem*, **386**, 194-216.
16. Mathews, D.H., Disney, M.D., Childs, J.L., Schroeder, S.J., Zuker, M. and Turner, D.H. (2004) Incorporating chemical modification constraints into a dynamic programming algorithm for prediction of RNA secondary structure. *Proc Natl Acad Sci U S A*, **101**, 7287-7292.
17. Zhang, D.Y. and Seelig, G. (2011) Dynamic DNA nanotechnology using strand-displacement reactions. *Nature Chemistry*, **3**, 103-113.

18. Curtis, E.A. and Bartel, D.P. (2001) The hammerhead cleavage reaction in monovalent cations. *RNA*, **7**, 546-552.
19. Chadalavada, D.M., Knudsen, S.M., Nakano, S. and Bevilacqua, P.C. (2000) A role for upstream RNA structure in facilitating the catalytic fold of the genomic hepatitis delta virus ribozyme. *J Mol Biol*, **301**, 349-367.
20. Jensen, K.K., Orum, H., Nielsen, P.E. and Norden, B. (1997) Kinetics for hybridization of peptide nucleic acids (PNA) with DNA and RNA studied with the BIAcore technique. *Biochemistry*, **36**, 5072-5077.
21. Navratilova, I., Eisenstien, E. and Myszka, D.G. (2005) Measuring long association phases using Biacore. *Anal Biochem*, **344**, 295-297.
22. Myszka, D.G. (2000) Kinetic, equilibrium, and thermodynamic analysis of macromolecular interactions with BIACORE. *Methods Enzymol*, **323**, 325-340.
23. Myszka, D.G. (1999) Improving biosensor analysis. *J Mol Recognit*, **12**, 279-284.